東北大学機関リポジトリ
TOUR
Tohoku University Repository

Application of Energy Dipersive Grazing Incidence X-ray Reflectometry Method to Structural Analysis of Liquid/Liquid and Liquid/Solid Interfaces

著者	Sato Shigeo, Imanaga Takuo, Matsubara Eiichiro, Saito Masatoshi, Waseda Yoshio
journal or publication title	Materials Transactions, JIM
volume	41
number	12
page range	1651-1656
year	2000
URL	http://hdl.handle.net/10097/52359

Materials Transactions, JIM, Vol. 41, No. 12 (2000) pp. 1651 to 1656
©2000 The Japan Institute of Metals

Application of Energy Dispersive Grazing Incidence X-ray Reflectometry Method to Structural Analysis of Liquid/Liquid and Liquid/Solid Interfaces

Shigeo Sato[1, *1], Takuo Imanaga[1, *2], Eiichiro Matsubara[2], Masatoshi Saito[1, *3] and Yoshio Waseda[1]

[1]*Institute for Advanced Materials Processing, Tohoku University, Sendai 980-8577, Japan*
[2]*Institute for Materials Research, Tohoku University, Sendai 980-8577, Japan*

The usefulness and validity of energy dispersive grazing incidence X-ray reflectometry (ED-GIXR) have been demonstrated for characterizing the liquid/liquid and liquid/solid interfaces. The present method appears to hold promise in reducing difficulty of conventional angular dispersive method due to absorption with an upper half liquid layer by enabling the use of high energy white X-ray radiation and obtaining much higher reflected intensity. An apparatus newly built for the exclusive use of the ED-GIXR is described with some selected examples of X-ray reflectivity profiles of solution/mercury and solution/electrode interfaces.

(Received June 9, 2000; Accepted November 2, 2000)

Keywords: *energy dispersive grazing incidence X-ray reflectometry, liquid/liquid interface, liquid/solid interface, mercury, electroplating*

1. Introduction

The liquid/solid and liquid/liquid interfaces are of fundamental importance from both the basic science and the applied engineering point of view. However, a few experimental data about structural information of such interfaces are available. We cite only some structural models of the liquid/liquid interfaces proposed from the thermodynamical point of view.[1)] The density variation across a vapor/liquid interface[2–4)] and the surface density, roughness and thickness of solid surface[5,6)] have been recently determined by the angular dispersive grazing incidence X-ray reflectometry (hereafter, referred to as AD-GIXR). This AD-GIXR technique can be, in principle, applied to the liquid/liquid and liquid/solid interfaces in order to obtain their reflectivity profiles. In practice, however, absorption of X-ray by a liquid layer above the interface is found to induce severe reduction of reflected X-ray intensity, and then it often prevents us to carry out the accurate reflectivity measurement. Consequently, the use of intense X-ray source of synchrotron radiation is essentially requested to measure the oil/water[7)] and electrolyte/electrode[8)] interfaces by AD-GIXR.

On the other hand, the energy dispersive grazing incidence X-ray reflectometry (hereafter, referred to as ED-GIXR) was recently applied to *in-situ* observations of thin film growth.[9,10)] In the ED-GIXR, a reflectivity intensity profile is obtained by a solid state detector as a function of incident X-ray energy. The absorption problem by the upper half liquid layer in the AD-GIXR can be solved by selecting higher energy white radiation in the ED-GIXR. In addition, the measurement time is shortened in the ED-GIXR, because no angular motion is required. These particular features in the ED-GIXR method prompt us to measure reflectivity profiles from liquid/solid and liquid/liquid interfaces using an in-house apparatus equipped with a rotating-anode X-ray generator without the use of synchrotron radiation.

The purpose of this paper is to describe the ED-GIXR apparatus newly built for measuring the liquid/solid and liquid/liquid interfaces, and its usefulness is shown by the results of X-ray reflectivity measurements for the solution/mercury and solution/Fe electrode interfaces.

2. Experimental

Schematic diagrams of the apparatus and the sample cell in the present ED-GIXR measurement are shown in Figs. 1(a) and (b), respectively. White X-ray is generated from a rotating tungsten anode operated with fine focus of 50 kV and 80 mA. The intensity distribution along the vertical direction is constant within about 12.0 mrad, which is much larger than the glancing angle α in the present measurement. The angle α with a horizontal liquid surface or a liquid/liquid interface is precisely adjusted by changing heights of two slits S_1 (0.04 mm) and S_2 (0.04 mm) placed on a tilting stage supported by two jackscrews a and b in Fig. 1(a). Similarly, the take-off angle of reflected beams α' is defined with a slit S_3 (0.02 mm) mounted on a stage supported by two jackscrews c and d. The height of the interface is also changed with another jackscrew e. The precision of the incident and reflected angles α and α' in this method is within $\pm 1.4 \times 10^{-3}$ mrad. In order to obtain a sufficiently flat mercury surface, the sample cell is set in 40 mm square. The cell is designed so as to penetrate the incident X-ray through a kapton window at one side of the wall and irradiate to the mercury surface or iron electrode completely immersed in solution. The reflected X-ray from the solution/mercury or solution/Fe electrode interface run through the solution and go out to the cell through another kapton window. The potential on the mercury or the iron electrode was controlled by the potentio-galvanostat through the

*1Present address: Inoue Superliquid Glass Project, ERATO.
*2Present address: Kawasaki Steel Techno-Research Corporation.
*3Present address: School of Health Sciences, Faculty of Medicine, Niigata University.

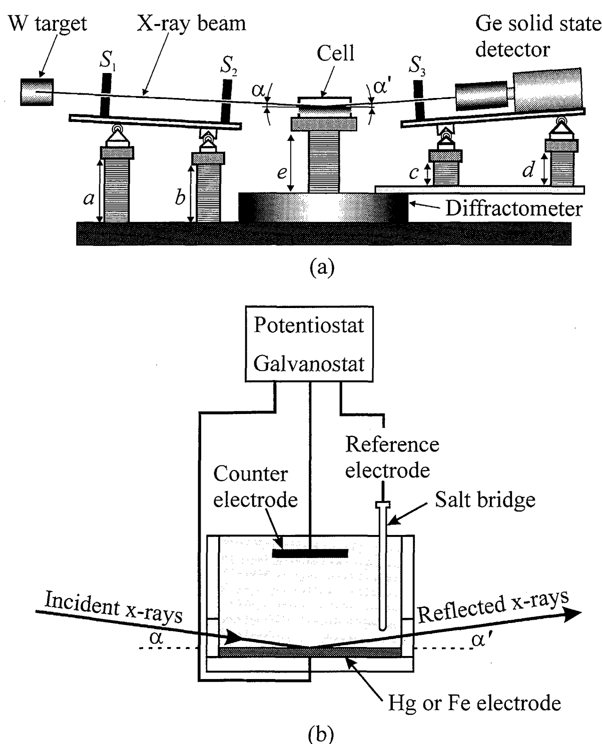

Fig. 1 (a) Schematic diagram of energy dispersive grazing incidence X-ray reflectometry (ED-GIXR) apparatus for a liquid surface or liquid-liquid interface. Jackscrews of a to d controls incident, α, and reflected angles, α'. (b) A sample cell.

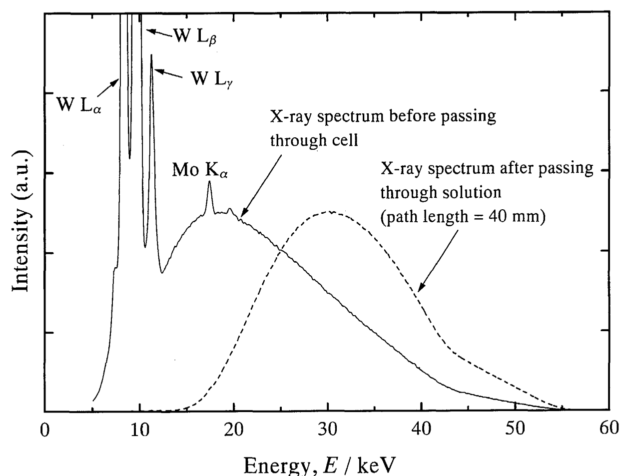

Fig. 2 The incident X-ray spectra from tungsten target before (solid line) and after (broken line) passing through water with path length of 40 mm.

Ag/AgCl standard electrode. Reflected X-ray is collected as a function of incident X-ray energy with a pure germanium solid state detector placed behind the slit S_3. In Fig. 2, the energy spectrum of the incident X-ray is compared with that of X-ray passing through 40 mm thick water layer. This thickness is equal to the distance of beam path of both incident and reflected X-rays through the water layer above the interface. As shown in Fig. 2, the original white X-ray includes some characteristic X-rays of tungsten and the contaminated molybdenum in the energy region less than 18 keV. However, such characteristic X-rays are almost completely absorbed by water. Thus, in the present measurement, the X-ray reflectivity profile is obtained from the energy spectrum above 20 keV.

For measuring one X-ray reflectivity profile, three spectra were collected. At first, the spectrum of the incident beam passing through solution was measured, similar to the case denoted by a broken line in Fig. 2. Secondly, the spectrum of reflected X-ray was obtained with respect to the surface or interface of interest. Thirdly, scattering intensity from solution alone was collected without mercury or iron electrode. The escape correction was carried out to all these spectra. The third spectrum is subtracted from the reflected X-ray spectrum so as to extract scattering from the surface or interface itself. The reflectivity profile as a function of energy can be obtained by dividing the corrected reflected intensity profile with that of the incident X-ray.

3. Results and Discussion

3.1 Evaluation of resolution for X-ray reflectivity measurement of ED-GIXR

Experimental resolution for scattering vector, $\boldsymbol{Q}$, in the energy dispersive method is known to be mainly limited by the energy resolution, ΔE, of a solid state detector, that is often the order of a few hundreds eV. On the other hand, the energy resolution can be converted to the angular resolution, $\Delta\theta$, by the following equation:

$$Q + \Delta Q = \frac{4\pi(E + \Delta E)}{hc}\sin\theta = \frac{4\pi E}{hc}\sin(\theta + \Delta\theta), \quad (1)$$

where h is the Planck's constant, c is the velocity of light and E is the energy of X-ray. Since the incident angle in the ED-GIXR method is the order of 1 mrad, the expected angular resolution converted from the energy resolution is found to be the order of 0.01 mrad. This is sufficiently enough for the resolution required in the present measurement. Good resolution of the reflectivity profile obtained in the ED-GIXR method has been confirmed by measuring the reflectivity from a 110 nm thick titanium film grown on a silicon wafer and comparing with the calculated curve. In this measurement, both angles α and α' were set at 1.92 mrad. The results are shown in Fig. 3, and good agreement between calculation and the experimental data is well recognized.

3.2 X-ray reflection from liquid/mercury interface

The reflectivity profile of a free mercury surface, that is, air/mercury interface is shown in Fig. 4. The angles α and α' were set at 2.09 mrad. The reflectivity profile obtained by the AD-GIXR method with Mo $K\alpha$[11] is also shown in Fig. 4 by converting the scale of degree to that of energy. There is a little discrepancy between two curves of ED-GIXR and AD-GIXR due to the energy dependence of X-ray absorption at the mercury surface and the difference of the angular resolution. However, we do not find any significant difference with respect to the critical point denoted by the critical energy of total reflection in these two independent results. This

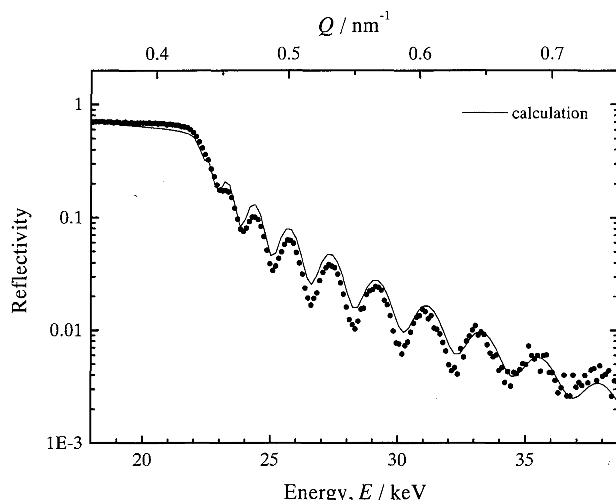

Fig. 3 X-ray reflectivity profiles of Ti(110 nm)/Si wafer measured with the ED-GIXR method (solid dot). The solid line corresponds to the calculated one.

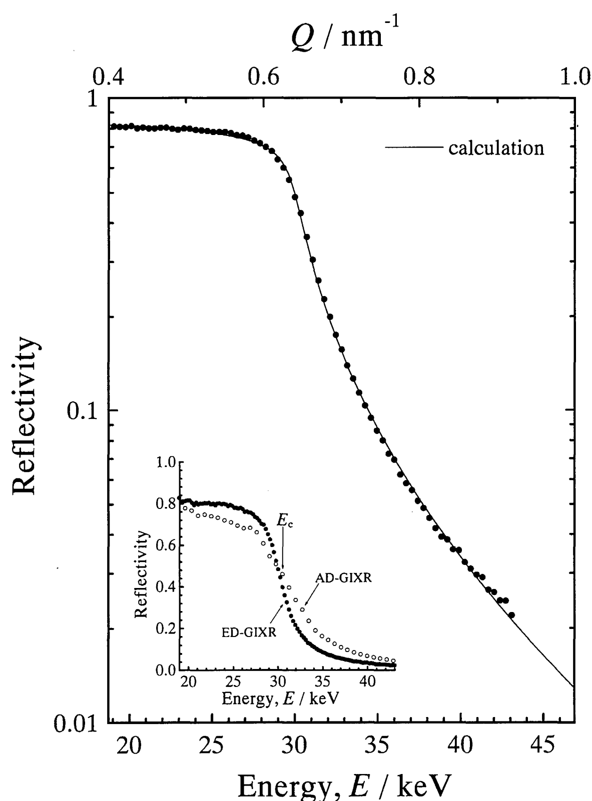

Fig. 4 X-ray reflectivity profile from free mercury surface. The solid dot and the solid line correspond to the experimental and calculated results, respectively. The inset represents the X-ray reflectivity altered in the linear scale. The open circle denotes the AD-GIXR data previously reported.[11]

suggests that the ED-GIXR method can provide information equivalent to the AD-GIXR method.

The experimental profile in Fig. 4 is fitted with the assumption of the root mean square roughness σ for the interface through the ratio $R(Q)/R_F(Q)$ of the experimental to the Fresnel reflectivity[2–4,7] in the following form:

$$\frac{R(Q)}{R_F(Q)} = \exp(-Q^2\langle\sigma^2\rangle). \tag{2}$$

The resultant value σ is 0.5 ± 0.1 nm for the free mercury surface. Considering that the value for the free mercury surface appears to be close to the value for water (H_2O) surface (0.32 nm) previously reported from the X-ray reflectivity measurement,[2] there is no significant difference in the density variation between the mercury and water surfaces. The density of free mercury surface, ρ, is calculated by the following equation:

$$\rho = \sqrt{2\delta(E_c)}, \tag{3}$$

where

$$\delta(E_c) = \frac{(hc)^2 r_e N_A}{2\pi E_c^2}\frac{Z_{mercury} + f'_{mercury}}{M_{mercury}}\rho_{mercury}, \tag{4}$$

where E_c is the critical energy for total reflection, r_e is the classical electron radius, N_A is the Avogadro's number, ρ is the density, Z is the Thomson scattering factor, f' is the real part of the anomalous dispersion factor, and M is atomic weight. From eqs. (3), (4) and the E_c of 30.40 keV, the density of free mercury surface is 12.20 Mg/m^3. The density obtained in this measurement is somewhat small compared with the bulk density of mercury at room temperature, 13.54 Mg/m^3. Although the definite origin of the difference cannot be certainly identified, it is quite likely that the top of mercury surface is oxidized to form mercury oxide such as HgO (11.19 Mg/m^3), because this measurement was conducted under air exposure. Considering the observed density of free mercury surface is intermediate density between mercury and HgO, the thickness of oxide layer is less than several tens nm, which is speculated by the penetration depth of X-ray under the grazing incident condition described in Sec. 3.3 in detail.

Similarly, the observed reflectivity profile of water/mercury interface is shown in Fig. 5. Because of absorption by water, the signals were collected for 12 ks, in order to keep good counting statistics. The variation of reflectivity below the critical point of total reflection is little. This is inconsistent with the results of our previous ED-GIXR data.[12] We must rather stress here that the present experimental results are not affected significantly by uncertainty in estimating the incident beam profile.

For estimating density of water/mercury surface from the critical energy of total reflection, a shift of the total reflection point is usually employed, because such shift can be given by a difference of refractive indices between water and air to mercury. The refractive index of mercury with substance of interest is explained as follows.

$$n = \sqrt{\frac{\varepsilon_{mercury}\mu_{mercury}}{\varepsilon_{sub}\mu_{sub}}} \approx \sqrt{\frac{\varepsilon_{mercury}}{\varepsilon_{sub}}} = \sqrt{\frac{\chi_{mercury}+1}{\chi_{sub}+1}}, \tag{5}$$

where ε, μ and χ is the dielectric constant, the magnetic permeability, the electric susceptibility in vacuum, respectively. Here, the subscript of *sub* denotes the substance set on the mercury surface. The electric permeability is expressed by

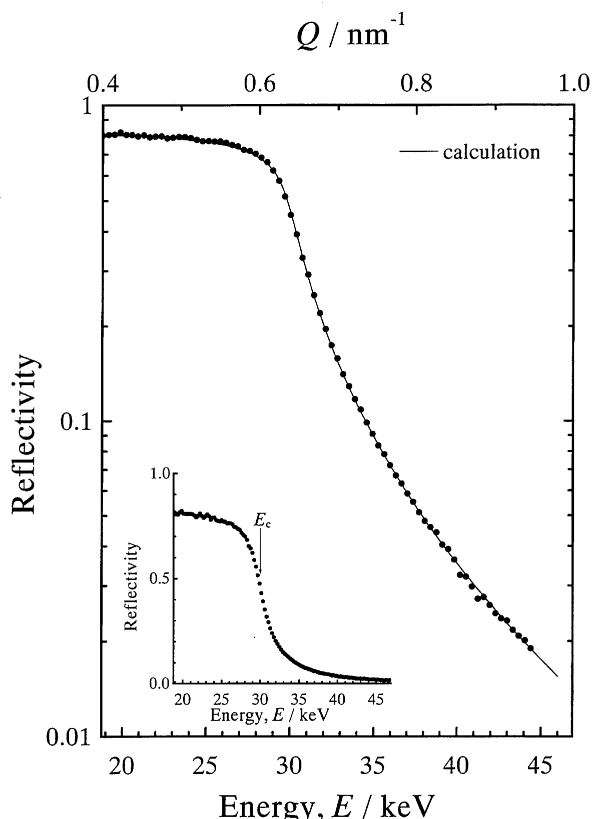

Fig. 5 X-ray reflectivity profiles from water/mercury interface (solid dot). The theoretical curve is shown with solid line. The inset represents the X-ray reflectivity altered in the linear scale.

$$\chi = -\frac{(hc)^2 r_e N_A \rho}{\pi E^2} \frac{\sum_j (Z_j + f'_j + i f''_j)}{\sum_j A_j}, \quad (6)$$

where j is the type of atom, and f'' is the imaginary part of the anomalous dispersion factor. The refractive index can also be written as follows:

$$n = 1 - \delta(E) - i\beta(E) \quad (7)$$

Since χ, $\delta(E)$ and $\beta(E)$ is extremely small, the following simplification is recognized.

$$n^2 = 1 + \chi_{mercury} - \chi_{sub} = 1 - 2\delta(E) - 2i\beta(E). \quad (8)$$

Thus, $\delta(E)$ can be expressed as follows:

$$\delta(E) = \frac{(hc)^2 r_e N_A}{2\pi E^2} \left(\frac{Z_{mercury} + f'_{mercury}}{A_{mercury}} \rho_{mercury} - \frac{\sum_j (Z_{sub,j} + f'_{sub,j})}{\sum_j A_{sub,j}} \rho_{sub} \right). \quad (9)$$

If the substance on mercury surface is air, the second term in a parenthesis of eq. (9) can be negligibly small. From eqs. (3) and (9) with the value (30.01 keV) of the critical energy of total reflection for water/mercury interface, the density of water/mercury interface is estimated to be 13.54 Mg/m^3, which is identical to the bulk density of mercury at room temperature. By fitting calculation to the experimental curve in Fig. 5, the root mean square roughness σ for water/mercury is estimated to be 0.4 ± 0.1 nm. This indicates that the interface thickness of water/mercury interface differs little from that (0.5 ± 0.1 nm) of free mercury surface.

Surface tension of mercury is known to change depending on its potential, and it is characterized by showing a maximum value at the electrocapillary maximum, E_{ecm}, where the mercury electrode is electrically neutral. This phenomenon is interpreted by taking into account of ionic adsorption in aqueous solution. Namely, the anions or cations adsorb on the electrode above or below E_{ecm}, respectively. The E_{ecm} for the mercury electrode in KCl (0.1 mol/l) aqueous solution is -0.704 V versus Ag/AgCl.[13] To investigate the effect of potential on the mercury surface, X-ray reflectivity measurements were carried out. Figure 6 shows the reflectivity profiles obtained under the different potential of 0.0, -0.7 and -1.5 V. From the calculation fit to the experimental data, the value of the root mean square roughness σ is estimated to be 0.4 ± 0.1 nm for the condition with potential of 0.0 and -0.7 V and 0.6 ± 0.1 nm for the case with potential of -1.5 V. Although we find a little difference in two cases, the present authors rather maintain the view that the applied potential to liquid mercury do not significantly affect on the interface thickness.

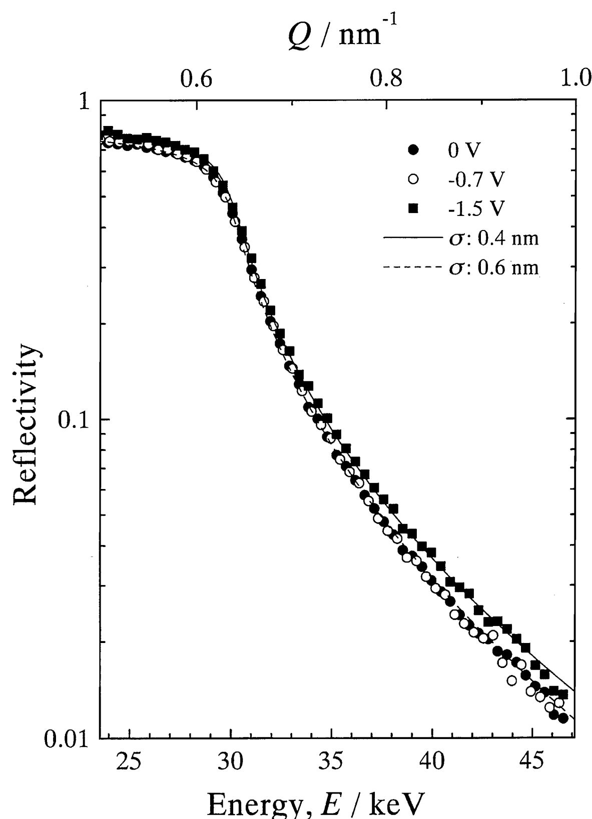

Fig. 6 X-ray reflectivity profiles of KCl (0.1 mol/l)/mercury interface. The X-ray reflectivity profiles given by solid dot, open circle and square denote the results measured by applying potential of 0.0, -0.7 and -1.5 V vs. Ag/AgCl on mercury, respectively.

3.3 *In-situ* observation of electroplating in solution by the ED-GIXR method

An attempt was also made in this work with respect to the *in-situ* observation of electroplating by ED-GIXR method. Iron polycrystalline electrode was prepared by mechanical polishing to optical flat. $NiSO_4$ aqueous solution of 0.01 mol/l was chosen to electroplate nickel on the electrode. Electroplating was made under galvanostatic electrolysis of −8.9 mA. The incident and reflection angles were fixed at 1.57 mrad for the present ED-GIXR measurements.

Figure 7 shows the reflectivity profiles of the $NiSO_4$ (0.1 mol/l)/Fe electrode interface observed after electroplating for zero, 300, 600 s. The critical energies for total reflection, E_c, after electroplating for zero, 300, 600 s are 32.0, 32.7 and 35.2 keV, respectively. The resultant surface density values for the cases with electroplating time of zero, 300 and 600 s are 7.7, 8.0 and 8.8 Mg/m^3, respectively. It may safely be said that the value for the first case (zero s) corresponds to the bulk density of iron (7.86 Mg/m^3). On the other hand, the value (8.8 Mg/m^3) for the 600 s case is close to the bulk density (8.85 Mg/m^3) of nickel. For convenience, the penetration depth of X-ray for nickel is illustrated in Fig. 8. This result suggests the penetration depth around the critical energy is several tens nm, and then the thickness of the 600 s case is estimated, at least, more than several nms. On the other hand, the surface density of the case with electroplating time of 300 s is smaller than the bulk density of nickel. This clearly indicates that the estimated density value corresponds to the mixed state of the upper nickel layer and the iron substrate. Finally, it should be mentioned that no oscillations (see Fig. 3) appear in the reflectivity profiles of Fig. 7 in spite of the existence of the nickel layer on the iron substrate. This is attributed to the rough surface of nickel layer.

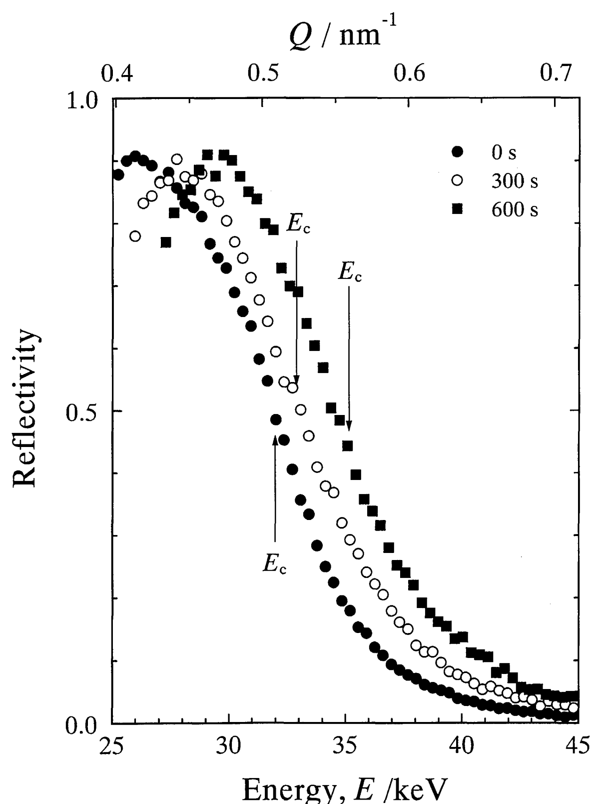

Fig. 7 X-ray reflectivity profiles of $NiSO_4$ (0.1 mol/l)/Fe electrode interface. The X-ray reflectivity profiles given by solid dot, open circle and square denote the results measured after electroplating for 0, 300 and 600 s, respectively.

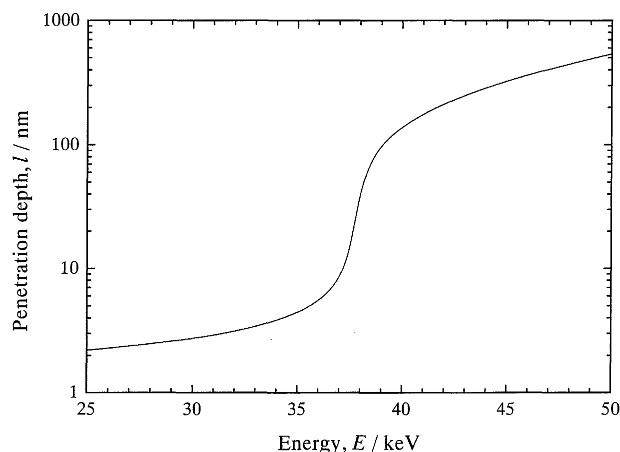

Fig. 8 The penetration depth of X-ray around the critical energy of total reflection for nickel.

4. Concluding Remarks

The usefulness and validity of ED-GIXR method for structural analysis of liquid surface, liquid/liquid and liquid/solid interfaces were tested by measuring the X-ray reflectivity profiles of thin solid film, solution/mercury and solution/electrode interfaces. The results are summarized as follows.

(1) The resolution of ED-GIXR method was evaluated by comparing the measured reflectivity curve of thin solid Ti film (110 nm) grown on a silicon wafer with the calculated one and was found to be sufficiently enough for the present purpose.

(2) By the high energy X-ray utilization, the X-ray reflection curves of liquid/mercury interfaces were obtained without the intense X-ray source of the synchrotron radiation.

(3) The thickness of transition zone between water and mercury could be estimated by evaluating X-ray reflectivity profiles, and this result suggests that the thickness of the transition zone of water/mercury interface is almost identical to that of the free mercury case.

(4) It was found that the ED-GIXR method can apply to the *in-situ* observation of density variation in the electroplating.

Taken from all results in this work, it would be very interesting to extend the ED-GIXR method to other systems of liquid/solid or liquid/liquid interfaces.

Acknowledgement

The authors would like to thank Prof. A. Inoue, Institute for Materials Research, Tohoku University, for his kind support.

REFERENCES

1) J. O'M. Bockris and A. K. N. Reddy: *Modern Electrochemistry*, Vol. 2, Plenum Press, New York, (1970), 718–791.
2) J. Als-Nielsen: Physica, **140A** (1986), 376–389.
3) A. Braslaw, M. Deutsch, P. S. Pershan, A. H. Weiss, J. Als-Nielsen and J. Boer: Phys. Rev. Lett., **54** (1985), 114–117.
4) M. K. Sanyal, S. K. Sinha, K. G. Huag and B. M. Ocko: Phys. Rev. Lett., **66** (1991), 628–631.
5) L. G. Parratt: Phys. Rev., **95** (1954), 359–369.
6) M. Saito, T. Kosaka, E. Matsubara and Y. Waseda: Mater. Trans., JIM, **36** (1995), 1–5.
7) B. R. McClain, D. D. Lee, B. L. Carvalho, S. G. J. Mochrie, S. H. Chen and J. D. Litster: Phys. Rev. Lett., **72** (1994), 246–249.
8) M. F. Toney, J. N. Howard, J. Richer, G. L. Borges, J. G. Gordon, O. R. Melroy, D. G. Wiesler, D. Yee and L. B. Sorensen: Surf. Sci., **335** (1995), 326–332.
9) E. Chason, T. M. Mayer and A. Payne: Appl. Phys. Lett., **60** (1992), 2353–2355.
10) K. Hayashi: Doctoral Thesis of Kyoto Univ., (1997).
11) S. Sato, M. Saito, E. Matsubara and Y. Waseda: Mater. Trans., JIM, **37** (1996), 1409–1412.
12) M. Saito, S. Sato and Y. Waseda: High Temp. Mater. and Processes, **17** (1998), 117–131.
13) D. C. Grahame: Chem. Rev., **41** (1947), 441–501.